Electronic Supplementary Material (ESI) for Journal of Materials Chemistry A.

Supporting Information

Isolated iron single-atom sites for oxygen reduction deriving from porphyrin-based carbon sphere by polymerization-coordination-pyrolysis strategy

Shengjie Wei,* Rongyan Yang, and Qinghua Zhang.

Experimental Section

Reagents: propionic acid (aladdin), benzene-1,4-dicarboxaldehyde (Acros), pyrrole (Innochem), N, N-dimethylformamide (DMF, Sinopharm Chemical), $FeCl_2 \cdot 4H_2O$ (www.xlhg.com), $CoCl_2 \cdot 6H_2O$ (Energy Chemical), $NiCl_2 \cdot 6H_2O$ (Sinopharm Chemical), Nafion D-521 dispersion (5% w/w in water and 1-propanol) (Alfa Aesar), commercial Pt/C (20 wt% metal, Alfa Aesar), KOH (analytical grade, Sinopharm Chemical). The distilled water used in ORR reaction was obtained through ion-exchange and filtration.

Preparation of porphyrin-based carbon sphere: 536 mg benzene-1,4-dicarboxaldehyde and 36 ml propionic acid were added in a 100 ml round-bottom flask and then were under ultrasonic treatment to form a homogeneous solution. Then, 533 μl pyrrole was added in the system. The round-bottom flask, which bottleneck was connected with a condenser tube, was heated to 142^{o}C in oil bath under vigorous stir for 7 hours. After reaction, the system was cooled to room temperature naturally. The obtained porphyrin-based carbon sphere was collected by centrifugation at 16,000 rpm for 10 min and washed by DMF for 3 times. Finally, the powder of porphyrin-based carbon sphere was dried at 80^{o}C in the oven.

Preparation of Fe-ISAS/CN: 130 μl 10 mg/ml $FeCl_2 \cdot 4H_2O$/DMF solution and 25 ml DMF were added in a round-bottom flask and were stirred for several minutes. Then, 100 mg the powder of porphyrin-based carbon sphere was added in the solution and was under ultrasonic treatment for several minutes. Then, the round-bottom flask,

which bottleneck was connected with a condenser tube, was heated to 160°C in oil bath under vigorous stir for 6 hours. After reaction, the system was cooled to room temperature naturally. The obtained Fe-coordinated porphyrin-based carbon sphere was collected by centrifugation at 16,000 rpm for 10 min and washed by DMF for 3 times and was dried at 80°C in the oven. Finally, the powder of Fe-coordinated porphyrin-based carbon sphere was transferred into a ceramic boat and was placed in a tube furnace. We heated the sample to 900°C with a heating rate of 5°C/min and kept the temperature for three hours under flowing nitrogen gas and then the sample was cooled naturally to room temperature.

Preparation of Co-ISAS/CN: 156 μl 10 mg/ml $CoCl_2 \cdot 6H_2O$/DMF solution and 25 ml DMF were added in a round-bottom flask and were stirred for several minutes. Then, 100 mg the powder of porphyrin-based carbon sphere was added in the solution and was under ultrasonic treatment for several minutes. Then, the round-bottom flask, which bottleneck was connected with a condenser tube, was heated to 160°C in oil bath under vigorous stir for 6 hours. After reaction, the system was cooled to room temperature naturally. The obtained Co-coordinated porphyrin-based carbon sphere was collected by centrifugation at 16,000 rpm for 10 min and washed by DMF for 3 times and was dried at 80°C in the oven. Finally, the powder of Co-coordinated porphyrin-based carbon sphere was transferred into a ceramic boat and was placed in a tube furnace. We heated the sample to 900°C with a heating rate of 5°C/min and kept the temperature for three hours under flowing nitrogen gas and then the sample was cooled naturally to room temperature.

Preparation of Ni-ISAS/CN: 156 μl 10 mg/ml $NiCl_2 \cdot 6H_2O$/DMF solution and 25 ml DMF were added in a round-bottom flask and were stirred for several minutes. Then, 100 mg the powder of porphyrin-based carbon sphere was added in the solution and was under ultrasonic treatment for several minutes. Then, the round-bottom flask, which bottleneck was connected with a condenser tube, was heated to 160°C in oil bath under vigorous stir for 6 hours. After reaction, the system was cooled to room temperature naturally. The obtained Ni-coordinated porphyrin-based carbon sphere was collected by centrifugation at 16,000 rpm for 10 min and washed by DMF for 3 times and was dried at 80°C in the oven. Finally, the powder of Ni-coordinated porphyrin-based carbon sphere was transferred into a ceramic boat and was placed in a tube furnace. We heated the sample to 900°C with a heating rate of 5°C/min and kept the temperature for three hours under flowing nitrogen gas and then the sample was cooled naturally to room temperature.

Preparation of CN: The powder of porphyrin-based carbon sphere was transferred into a ceramic boat and was placed in a tube furnace. We heated the sample to 900°C with a heating rate of 5°C/min and kept the temperature for three hours under flowing nitrogen gas and then the sample was cooled naturally to room temperature.

Characterization

The crystalline structure and phase purity was measured by utilizing Rigaku RU-200b X-ray powder diffractometer (XRD) with CuKα radiation (λ= 1.5418Å). We analyzed the metal concentrations of the samples by inductively coupled plasma

optical emission spectrometry (ICP-OES). STEM observation was performed by using a probe aberration-corrected microscope, JEM-ARM200F equipped with a cold emitter, operated at 200kV. The microscope has an attainable spatial resolution of 78pm. The atomic structure of the samples were characterized using an ARM-200CF (JEOL, Tokyo, Japan) transmission electron microscope operated at 200 keV and equipped with double spherical aberration (Cs) correctors. The attainable resolution of the probe defined by the objective pre-field is 78 picometers.

XAFS measurement: We performed the X-ray absorption fine structure measurement at 1W1B station in Beijing Synchrotron Radiation Facility (BSRF) for Fe K-edge, Co K-edge, and Ni K-edge. The XAFS data was measured at room temperature in fluorescence mold by using ionization chamber. We pelletized all the powder of samples as a disks with a diameter of 8 mm by utilizing polyvinylidene fluoride (PVDF) powder serving as binders and all spectra were collected in ambient conditions.

XAFS Analysis and Results: The obtained EXAFS data were analyzed according to the standard procedures by the analysis of the ATHENA module of the IFEFFIT software packages. The obtained EXAFS spectra were treated by subtracting post-edge background from the overall absorption and normalizing according to the edge-jump step. Then, the $\chi(k)$ data was transformed to real (R) space by utilizing a hanning windows (dk=1.0 $Å^{-1}$) in order to separate the EXAFS contributions from different coordination shells. We carried out Least-squares curve parameter fitting by

using the ARTEMIS module of the IFEFFIT software packages to obtain the quantitative structural parameters around central metal atom.[1]

The EXAFS equation was listed below:

$$\chi(k)=\sum_{j}\frac{N_j S_o^2 F_j(k)}{kR_j^2}\exp[-2k^2\sigma_j^2]\exp[\frac{-2R_j}{\lambda(k)}]\sin[2kR_j+\phi_j(k)]$$

In the above equation, S_0^2 indicated the amplitude reduction factor. $F_j(k)$ was the effective curved-wave backscattering amplitude. N_j indicated the number of neighbors in the j^{th} atomic shell. R_j was the distance between the X-ray absorbing central atom and the atoms in the j^{th} atomic shell (backscatterer). λ indicated the mean free path in Å. σ_j represented the Debye-Waller parameter of the j^{th} atomic shell (variation of distances around the average R_j). $\phi_j(k)$ was the phase shift (including the phase shift for each shell and the total central atom phase shift). The functions $F_j(k)$, λ and $\phi_j(k)$ were calculated with the ab initio code FEFF8.2.[2] The additional details for EXAFS simulations were exhibited below.

The S_0^2 value was 0.85 and the value was fixed in the subsequent fitting of Fe, Co and Ni K-edge, while the internal atomic distances R, the edge-energy shift ΔE_0 and Debye-Waller factor σ^2 were allowed to work separately. The obtained parameters of Fe, Co and Ni K-edge were exhibited in Table S2.

Electro-catalytic Measurement

All catalysts were prepared by mixing 10 mg of the catalyst in 1 ml of solution which contained 490 μL of ethanol, 490 μL of H_2O and 20 μL of 5% Nafion solution. Then, the solution was under ultrasonic treatment for 1 h to obtain homogeneous catalyst inks. We prepared the commercial 20 wt% Pt/C catalysts inks by the similar treatment and the concentration of commercial 20 wt% Pt/C was 5mg/ml. 30 μl Fe-ISAS/CN and CN catalysts inks and 5 μl commercial 20 wt% Pt/C catalysts inks were carefully dropped on the polished glassy carbon rotating disk electrode (RDE) or rotating ring disk electrode (RRDE) to assure that the electrode was fully covered. For ORR measurement, the catalyst loading of Fe-ISAS/CN is 1.53 mg/cm^2 with 5.5 μg Fe/cm^2 for ORR. While the catalyst loading of 20 wt% Pt/C is 0.13 mg/cm^2 with 26 μg Pt/cm^2 for ORR.

The electrochemical measurements were performed by using a three-electrode system on a CHI 760E electrochemical workstation (Shanghai Chenhua, China) in 0.1 M KOH electrolyte. A rotating disk electrode (RDE) with a glassy carbon (GC) disk of 5 mm in diameter and a rotating ring-disk electrode with a Pt ring (6.5 mm inner diameter and 8.5 mm outer diameter) were chosen as the working electrode. A carbon rod was utilized as counter electrode. The potential was recorded by utilizing a Ag/AgCl (saturated KCl solution) electrode as the reference electrode. Prior to electrochemical measurement, we passed oxygen flow through the electrolyte in the cell for at least 30 minutes to assure the solution was saturated with O_2, and all electrochemical experiments were performed at room temperature. We measured

Linear sweep voltammetry (LSV) measurements at various rotating speed from 400 to 2500 rpm with a scan rate of 10 $mV \cdot s^{-1}$, and the cyclic voltammetry (CV) experiments were carried out with a scan rate of 50 $mV \cdot s^{-1}$.

For the ORR at a RDE, we calculated the electron transfer number (n) and kinetic current density (J_k) according to the Koutecky-Levich equation as below:

$$\frac{1}{J} = \frac{1}{J_L} + \frac{1}{J_K} = \frac{1}{B\omega^{\frac{1}{2}}} + \frac{1}{J_K} \quad (1)$$

$$\mathrm{B} = 0.62\mathrm{nF}C_0\, D_0^{\frac{2}{3}} V^{-\frac{1}{6}} \quad (2)$$

In the above equation, J was the measured current density, J_K and J_L represented the kinetic and limiting current densities, respectively. ω indicated the angular velocity of the disk. n and F were the electron transfer number and the Faraday constant, respectively, and the value of Faraday constant was 96485 $C \cdot mol^{-1}$. C_0, D_0 and V were the bulk concentration of O_2 (1.2×10^{-6} $mol \cdot cm^{-3}$), the diffusion coefficient of O_2 (1.9×10^{-5} $cm^2 \cdot s^{-1}$), and the kinematic viscosity of the electrolyte (0.01 $cm^2 \cdot s^{-1}$), respectively.

During the hydrogen peroxide yield tests, the disk electrode of RRDE was scanned catholically at a rate of 10 $mV \cdot s^{-1}$ and the ring electrode potential was set to 1.23 V vs. RHE. The hydrogen peroxide yield (H_2O_2%) and the electron transfer number (n) can be calculated by utilizing the equations as below:

$$H_2O_2\,(\%) = 200 \times \frac{\frac{I_r}{N}}{I_d + \frac{I_r}{N}} \quad (3)$$

$$\mathrm{n} = 4 \times \frac{I_d}{I_d + \frac{I_r}{N}} \quad (4)$$

In the above equation, I_r and I_d represented the ring current and disk current, respectively. N represented the current collection efficiency of the Pt ring and its value was 0.4.

The durability tests of the catalysts were performed in the O_2-saturated 0.1 M KOH electrolyte at room temperature by performing potential cycling between 0.6 and 1.0 V vs. RHE. at a sweep rate of 50 $mV \cdot s^{-1}$ for 5,000 cycles.

Zinc-air battery Measurements

A home-made Zn-air battery device was designed during the measurements and stability tests. 6 M KOH aqueous solution served as the electrolyte for Zn-air battery device and the electrolyte was cycled by a circulating pump. A polished zinc plate was utilized as the anode and a certain volume of catalyst ink was brushed onto a 4 cm^2 carbon paper (HCP030) as cathode. The cathode material is composed of Ni foam (bottom), Gas Diffusion and Waterproof Layer (middle) and Carbon paper (top). The catalyst loading of Fe-ISAS/CN was 2 mg/cm^2 with 7 μg Fe/cm^2. The catalyst loading of commercial 20 wt% Pt/C was 0.5 mg/cm^2 with 100 μg Pt/cm^2.

During galvanostatic charge and discharge measurement at 10 mA/cm^2, 6 M KOH/0.2 M $Zn(CH_3COO)_2$ served as the electrolyte. The catalysts loading were 2 mg/cm^2 Fe-ISAS/CN and 0.2 mg/cm^2 RuO_2.

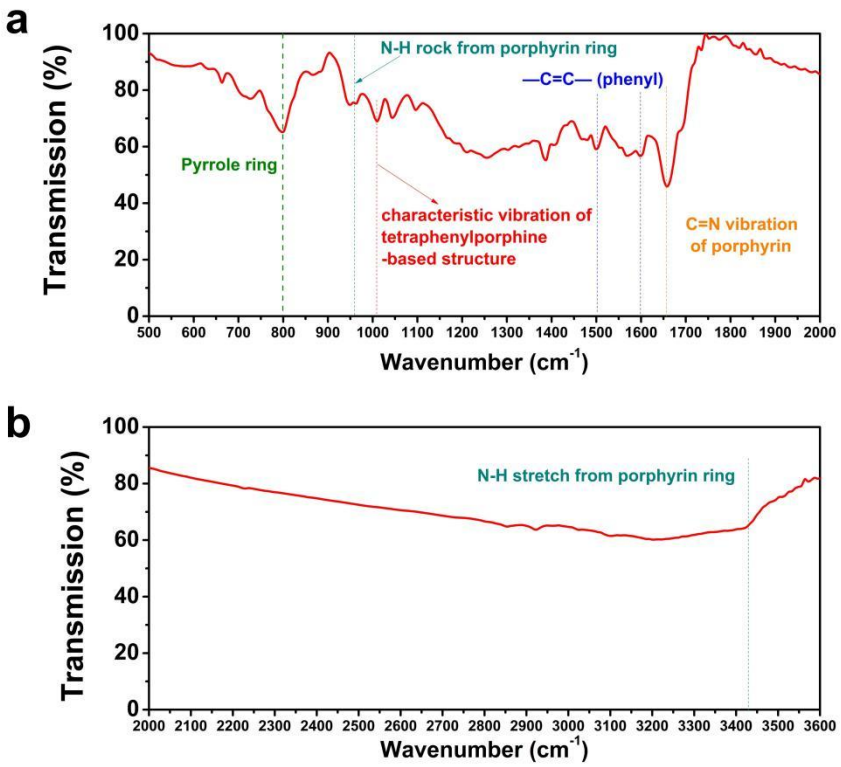

Figure S1. The FTIR pattern of the synthesized porphyrin carbon spheres.

The strong absorption band near 1000 cm^{-1} is ascribed to the characteristic vibration of the tetraphenylporphine-based structure (*J. Am. Chem. Soc.*, 1959, **81**, 5111), demonstrating the successful construction of tetraphenylporphine-based framework. The absorption bands around 960 cm^{-1} and 3430 cm^{-1} are ascribed to N-H rocking vibration and N-H stretching vibration from porphyrin ring, respectively (*J. Am. Chem. Soc.*, 1959, **81**, 5111). The strong absorption band around 1660 cm^{-1} is ascribed to C=N stretching vibration of porphyrin ring (*Adv. Mater.*, 2019, **31**, 1900592). The strong absorption band around 800 cm^{-1} is from pyrrole ring (*J. Am. Chem. Soc.*, 1959, **81**, 5111). The two absorption bands around 1500 cm^{-1} and 1600 cm^{-1} are from C=C stretching vibration of phenyl (*J. Am. Chem. Soc.*, 1959, **81**, 5111). Therefore, the existence of the characteristic absorption band from tetraphenylporphine-based structure, the absorption bands of N-H vibration and the absorption band of C=N stretching vibration from porphyrin ring demonstrates the successful synthesis of porphyrin-based structure.

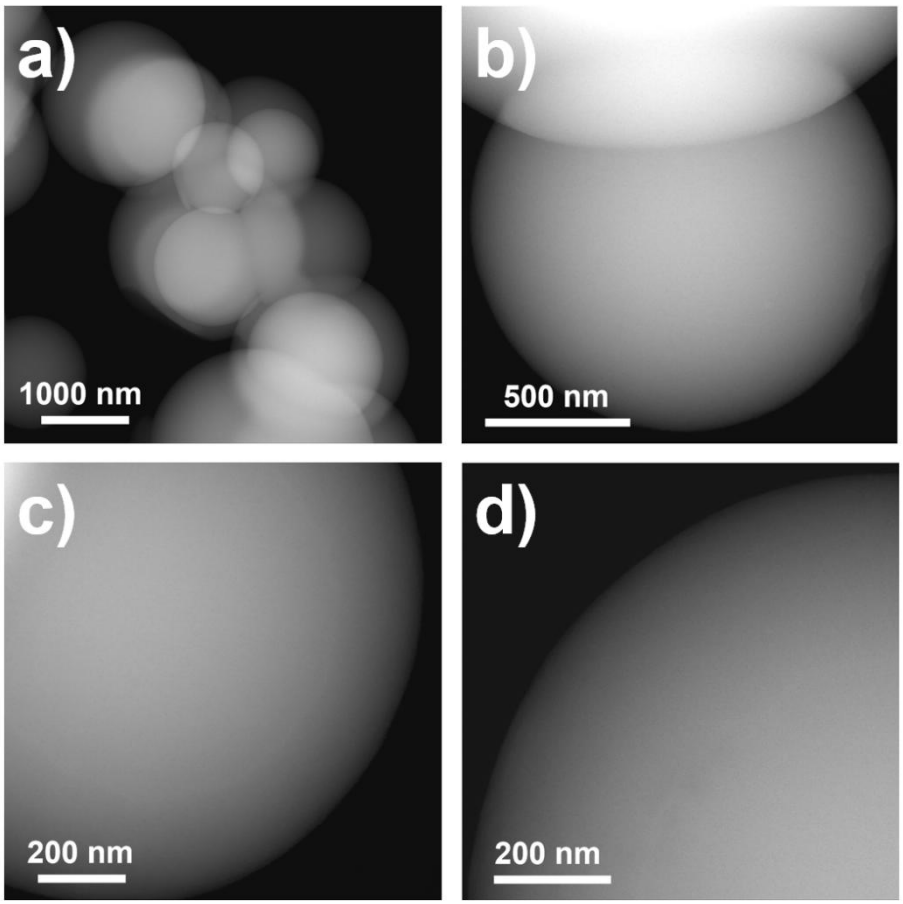

Figure S2. a) - d), The HAADF-STEM images of Fe-ISAS/CN from different regions at different magnifications.

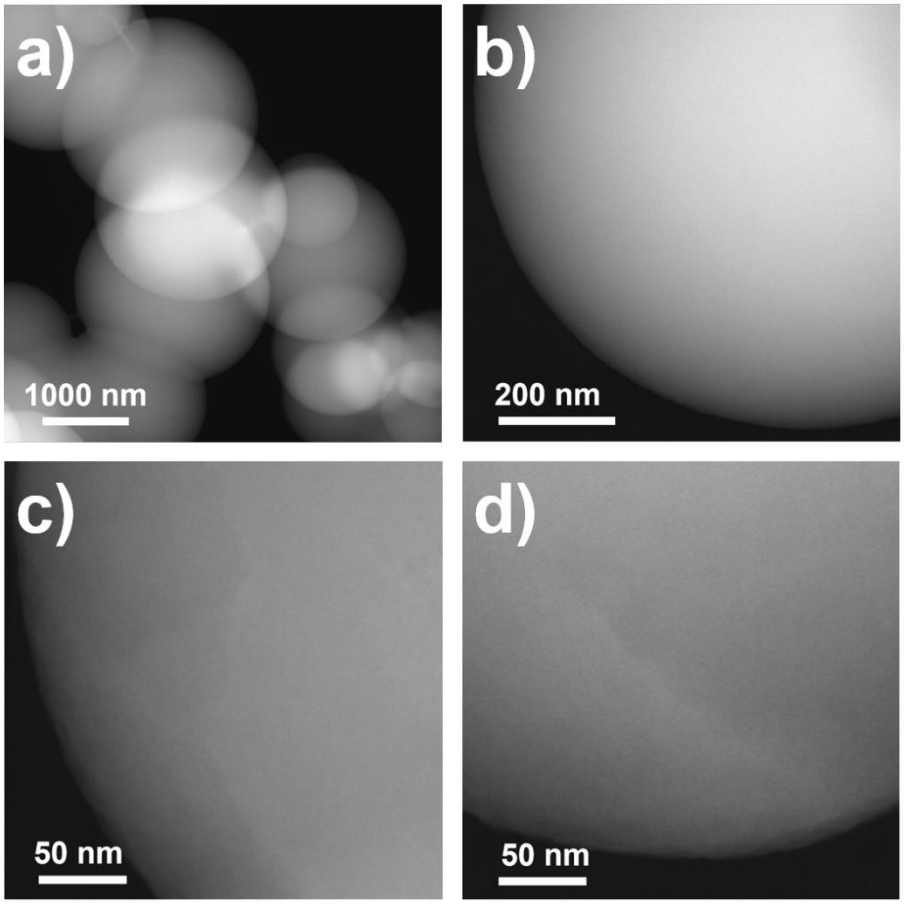

Figure S3. a) - d), The HAADF-STEM images of Co-ISAS/CN from different regions at different magnifications.

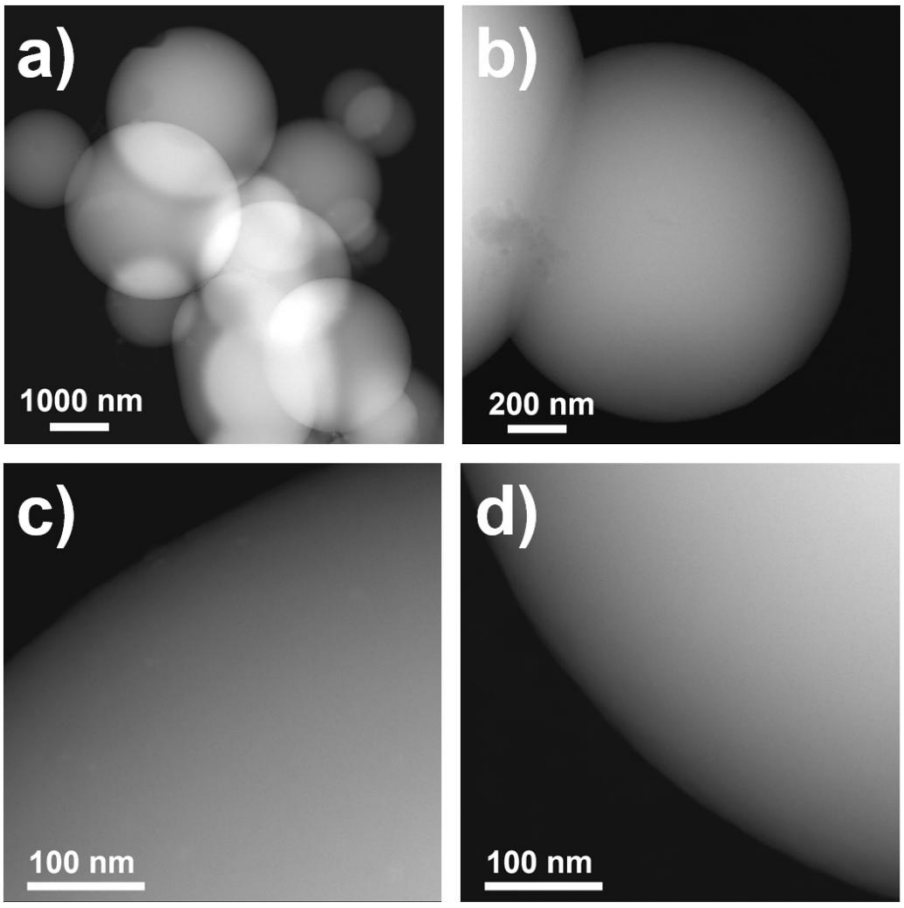

Figure S4. a) - d), The HAADF-STEM images of Ni-ISAS/CN from different regions at different magnifications.

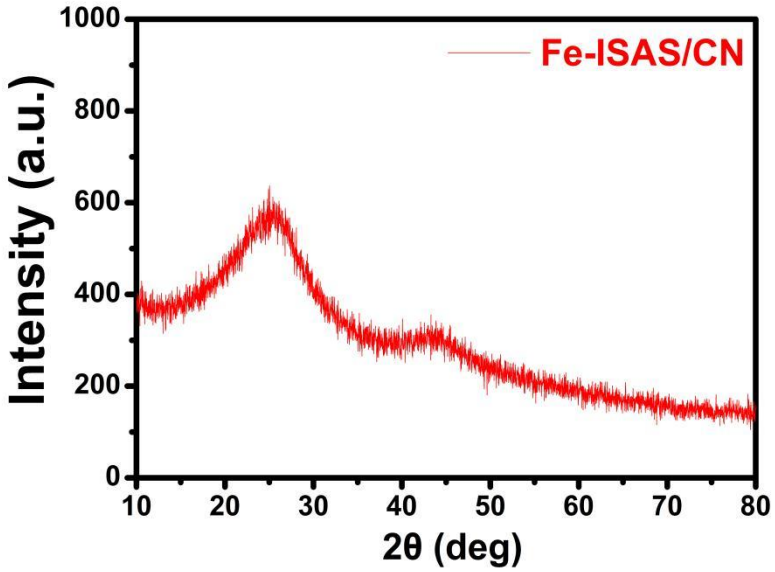

Figure S5. The XRD pattern of Fe-ISAS/CN.

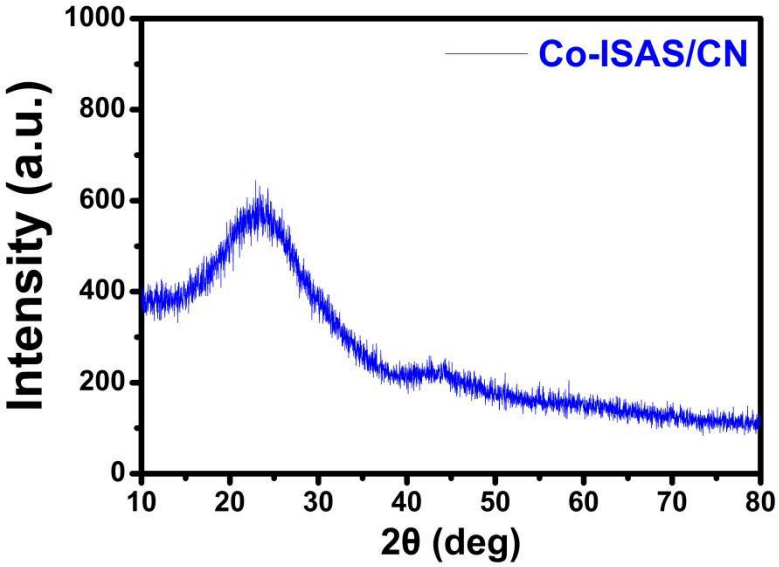

Figure S6. The XRD pattern of Co-ISAS/CN.

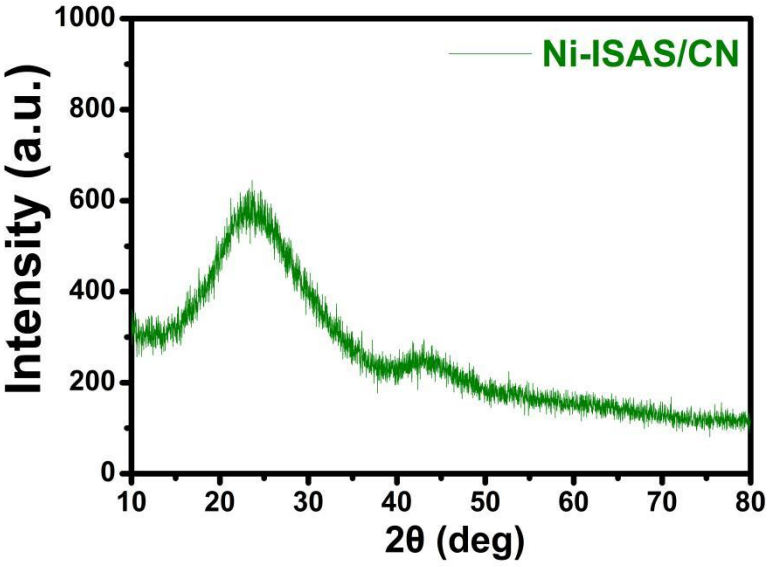

Figure S7. The XRD pattern of Ni-ISAS/CN.

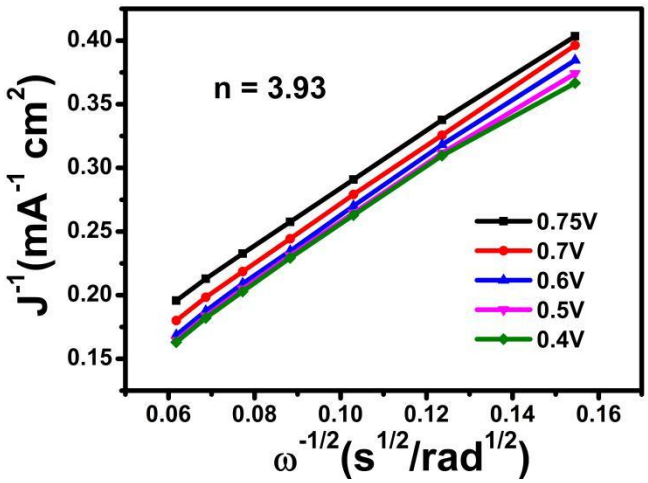

Figure S8. The electron transfer number of Fe-ISAS/CN for ORR.

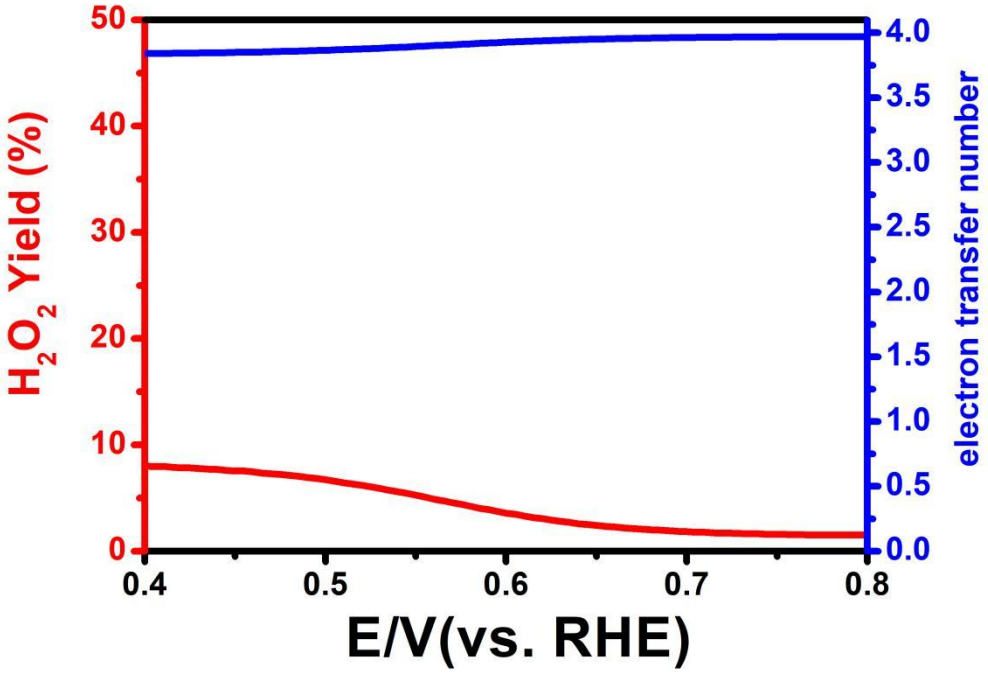

Figure S9. The H_2O_2 yield and corresponding electron transfer number of Fe-ISAS/CN for ORR in the O_2-saturated 0.1 M KOH solution.

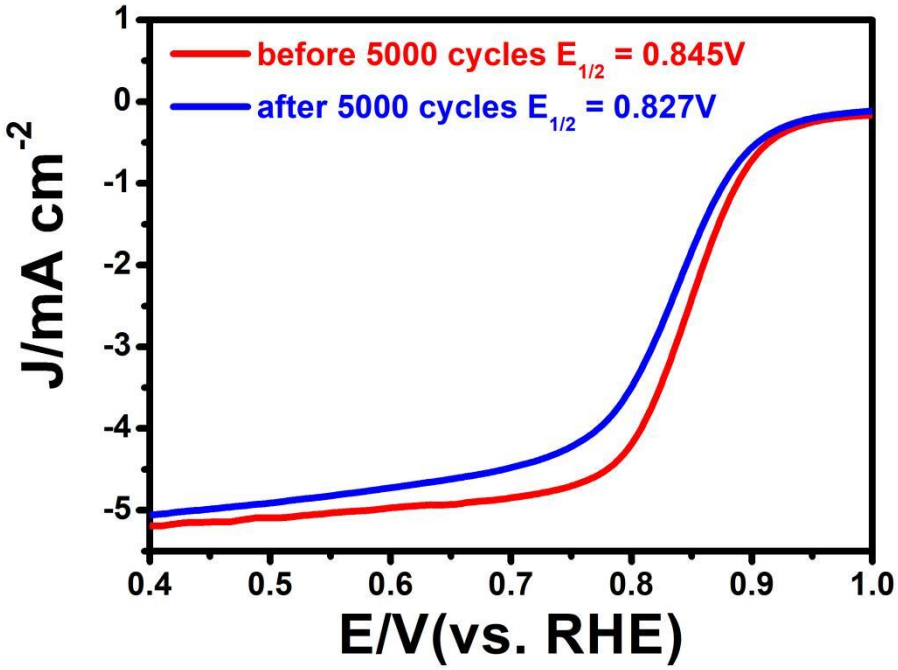

Figure S10. The comparison between the catalytic performance of commercial 20 wt% Pt/C during the stability test in ORR reaction before and after 5000 cycles.

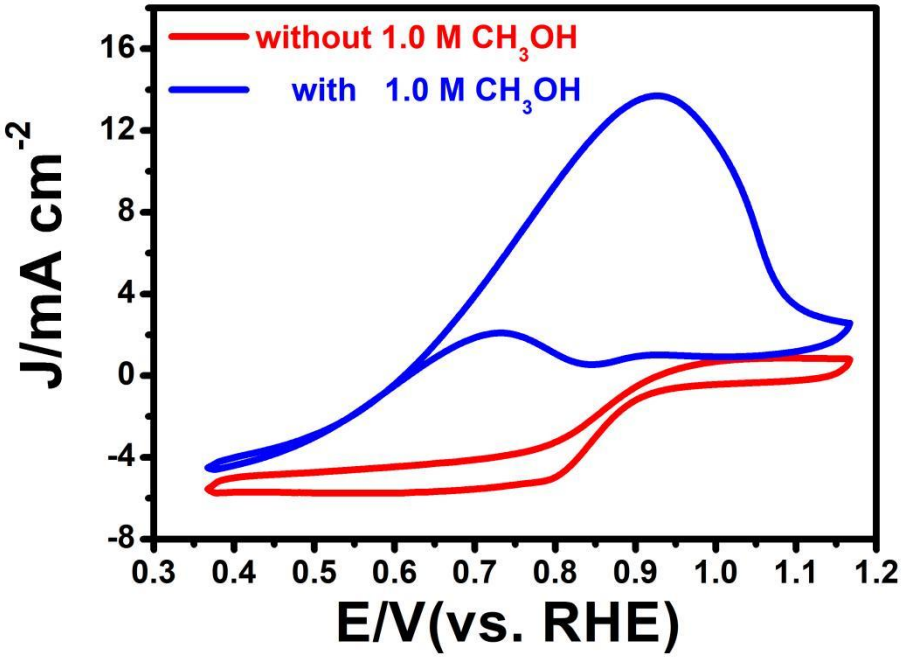

Figure S11. The comparison of CV curves of commercial 20 wt% Pt/C in O_2-saturated 0.1 M KOH without and with 1.0 M CH_3OH at a scan rate of 50 mV/s.

Table S1 Inductively coupled plasma optical emission spectrometry (ICP-OES) measurements of metal-ISAS/CN.

Sample	The metal content (wt%)
Fe-ISAS/CN	0.36
Co-ISAS/CN	0.31
Ni-ISAS/CN	0.33

Table S2. Structural parameters extracted from the Fe, Co and Ni K-edge EXAFS fitting. (S_0^2=0.85)

Sample	Scattering pair	CN	R(Å)	σ^2(10^{-3} Å^2)	ΔE_0(eV)	R factor
Fe-ISAS/CN	Fe-N/C	4.1	2.01	6.4	1.5	0.006
Co-ISAS/CN	Co-N/C	3.9	1.99	7.3	-2.0	0.003
Ni-ISAS/CN	Ni-N/C	4.2	1.92	6.5	-1.5	0.005

The meaning of S_0^2 was the amplitude reduction factor; CN was the coordination number; R represented interatomic distance (the bond length between central atoms and surrounding coordination atoms); σ^2 indicated Debye-Waller factor (a measure of thermal and static disorder in absorber-scatterer distances); ΔE_0 was edge-energy shift (the difference between the zero kinetic energy value of the sample and that of the theoretical model). R factor was used to evaluate the goodness of the fitting. Error bounds which characterized the structural parameters obtained by EXAFS spectroscopy were estimated as N ± 20%; R ± 1%; σ^2 ± 20%; ΔE_0 ± 20%.

Table S3. The comparison of ORR catalytic performance between Fe-ISAS/CN and other reported non-precious electrocatalysts.

electrocatalysts	$E_{1/2}$ (V vs. RHE)	reference
Fe-ISAS/CN	0.881	This work
Fe_H-N-C	0.91	*Adv. Mater.*, 2023, **35**, 2210714.
Co-CMS	0.83	*Adv. Energy Mater.*, 2022, **12**, 2103097.
Fe_1/d-CN	0.950	*Energy Environ. Sci.*, 2021, **14**, 6455.
Fe,Mn/N-C	0.928	*Nat. Commun.*, 2021, **12**, 1734.
S-Co/N/C	0.86	*ACS Catal.*, 2021, **11**, 4498.
Co@N-C700	0.78	*Chem. Eng. J.*, 2021, **421**, 129719.
FeNi SAs/NC	0.84	*Adv. Energy Mater.*, 2021, **11**, 2101242.
FeSA-N-C	0.9	*Nat. Commun.*, 2020, **11**, 2831.
Mg-N-C	0.910	*Nat. Commun.*, 2020, **11**, 938.
Fe-NC-S	0.88	*Chem*, 2020, **6**, 3440.
Fe-N/P-C-700	0.867	*J. Am. Chem. Soc.*, 2020, **142**, 2404.
Co SAs/3D GFs	0.901	*Angew. Chem. Int. Ed.*, 2020, **59**, 20465.
Fe-NiNC	0.84	*Nano Energy*, 2020, **71**, 104597.
Co-FeCo/N-G	0.82	*Appl. Catal. B*, 2019, **256**, 117887.
Fe-N-C HNSs	0.87	*Adv. Mater.*, 2019, **31**, 1806312.
Fe-SAs/NPS-HC	0.912	*Nat. Commun.*, 2018, **9**, 5422.
Fe SAs-N/C-20	0.909	*J. Am. Chem. Soc.*, 2018, **140**, 11594.
p-Fe-N-CNFs	0.82	*Energy Environ. Sci.*, 2018, **11**, 2208.
Fe2-Z8-C	0.871	*Angew. Chem. Int. Ed.*, 2018, **57**, 1204.
Fe-N-DSC	0.84	*ACS Nano*, 2018, **12**, 208.
FeSAs/PTF-600	0.87	*ACS Energy Lett.*, 2018, **3**, 883.
Fe-N_4 SAs/NPC	0.885	*Angew. Chem. Int. Ed.*, 2018, **57**, 8614.

Table S4. The comparison of the peak power density for Zn-air battery between Fe-ISAS/CN and other reported non-noble metal-based catalysts.

catalyst	Peak power density (mW/cm^2)	Reference
Fe-ISAS/CN	81.8	This work
Fe-Se/NC	135	*Angew. Chem. Int. Ed.*, 2023, **62**, e202219191.
3D SAFe	156	*Nano Lett.*, 2022, **22**, 7386.
MS-CoSA-N-C-800°C	160	*ACS Nano*, 2022, **16**, 11944.
V-Co_3O_4	40.6	*ACS Catal.*, 2021, **11**, 8097.
FeCo/Se-CNT	37.5	*Nano Lett.*, 2021, **21**, 2255.
Fe_1/d-CN	78	*Energy Environ. Sci.*, 2021, **14**, 6455.
FeNiCo@NC-P	112	*Adv. Funct. Mater.*, 2020, **30**, 1908167.
FeP/Fe_2O_3@NPCA	40.8	*Adv. Mater.*, 2020, **32**, 2002292.
Fe-N/P-C-700	133.2	*J. Am. Chem. Soc.*, 2020, **142**, 2404.
SA-PtCoF	125	*Energy. Environ. Sci.*, 2020, **13**, 884.
pfSAC-Fe-0.2	126.83	*Sci. Adv.*, 2019, **5**, eaaw2322.
Co-POC	78	*Adv. Mater.*, 2019, **31**, 1900592.
co-doped np-graphene	83.8	*Adv. Mater.*, 2019, **31**, 1900843.
CAN-Pc(Fe/Co)	88	*Angew. Chem. Int. Ed.*, 2019, **58**, 14724.
CoNi-SAs/NC	101.4	*Adv. Mater.*, 2019, **31**, 1905622.
Co-SAs@NC	105.3	*Angew. Chem. Int. Ed.*, 2019, **58**, 5359.
NC-Co SA	20.9	*ACS Catal.*, 2018, **8**, 8961.

Supplementary References

[1] B. Ravel, M. Newville, *J. Synchrotron Radiat.*, 2005, **12**, 537-541.

[2] A. L. JAnkudinov, B. Ravel, J. J. Rehr, S. D. Conradson, *Phys. Rev. B*, 1998, **58**, 7565-7576.